Optimal circular dichroism sensing with quantum light: Multiparameter estimation approach

Christina Ioannou [ORCID],[1] Ranjith Nair [ORCID],[2,3] Ivan Fernandez-Corbaton [ORCID],[4] Mile Gu [ORCID],[2,3,5] Carsten Rockstuhl,[1,4] and Changhyoup Lee [ORCID][1,6,*]

[1]*Institute of Theoretical Solid State Physics, Karlsruhe Institute of Technology, 76131 Karlsruhe, Germany*
[2]*School of Physical and Mathematical Sciences, Nanyang Technological University, Singapore 637371, Singapore*
[3]*Complexity Institute, Nanyang Technological University, Singapore 637460, Singapore*
[4]*Institute of Nanotechnology, Karlsruhe Institute of Technology, 76021 Karlsruhe, Germany*
[5]*Centre for Quantum Technologies, National University of Singapore, Singapore 117543, Singapore*
[6]*Quantum Universe Center, Korea Institute for Advanced Study, Seoul 02455, Republic of Korea*

The measurement of circular dichroism (CD) has widely been exploited to distinguish the different enantiomers of chiral structures. It has been applied to natural materials (e.g., molecules) as well as to artificial materials (e.g., nanophotonic structures). However, especially for chiral molecules the signal level is very low and increasing the signal-to-noise ratio is of paramount importance to either shorten the necessary measurement time or to lower the minimum detectable molecule concentration. As one solution to this problem, we propose here to use quantum states of light in CD sensing to reduce the noise below the shot noise level encountered when using coherent states of light. Through a multiparameter estimation approach, we identify the ultimate quantum limit of the precision in CD sensing, allowing for general schemes including additional ancillary modes. We show that the ultimate quantum limit can be achieved by various optimal schemes. These include using a pair of Fock-state probes in a direct sensing configuration and pairs of twin beams in an ancilla-assisted sensing configuration, for both of which photon number-resolved detection is shown to be the optimal measurement. These optimal schemes offer a significant quantum enhancement even in the presence of some additional system loss. The near optimality of a scheme using a single twin beam in a direct sensing configuration is also shown for cases where the actual CD signal is very small. Alternative optimal schemes involving single-photon sources and detectors are also proposed. This work paves the way for further investigations of quantum metrological techniques in chirality sensing.

I. INTRODUCTION

Measuring the optical response of media that consist of either chiral molecules [1,2] or chiral nanophotonic structures [3–5] is of great importance in various scientific fields, from fundamentals to applications [6,7]. The chiral properties of a medium or a structure cause an asymmetric optical response upon illumination with left- (LCP, or L) and right-handed circularly polarized (RCP, or R) light beams. An electric-magnetic coupling can explain the induced optical effects such as circular dichroism (CD) and optical rotation [8,9]. While the former expresses the difference in absorption between LCP and RCP, the latter expresses a different phase accumulation upon propagation, leading to the rotation of the plane of linear polarization of the light beam.

The measurement of the CD signal has in particular been widely used in various fields over the last few decades due to the simplicity of the measurement scheme combined with the rich information contained in the CD signal [1,2]. CD sensing refers to the estimation of interesting sample parameters as a function of the outcomes of CD measurement. Despite the great importance of CD sensing, the CD signal is usually very weak (the relative differential absorbance is $\sim 10^{-3}$ to 10^{-5} for chiral molecules) in realistic scenarios [10]. CD is a nonlocal optical effect of the lowest order and only happens for molecules with broken inversion symmetry. Since the spatial extent of most molecules with respect to the incident beam is negligibly small, the overall effect is rather tiny. When measuring it, one often struggles against the noise level, similar to the case of gravitational wave detectors [11,12]. This limits the usefulness of CD spectroscopy to cases where molecules are present either in high concentrations or in large volumes [13,14], so that it is possible to accumulate enough signal.

An obvious solution to the problem would be to increase the intensity of light that is incident on the analyte. However, this is not always an option due to optical damage that may occur in some situations [15–18]. Hence, one needs to look for alternative means to improve the sensing performance while keeping the incident power in the low-intensity regime. One way to enhance the CD signal for a fixed light source is to use supporting photonic nanostructures [6,19–23] or optical cavities [24].

A fundamentally different approach would be to use quantum states of light for sensing chiral properties of molecules. Quantum sensing schemes, in general, can reduce the noise

---

*changhyoup.lee@gmail.com

below the shot-noise limit and consequently improve the signal-to-noise-ratio. For example, optical activity and optical rotatory dispersion of sucrose solution have been measured using single photons [25] and polarization-entangled states [26], respectively. Both experimental studies clearly demonstrated the quantum enhancement in the estimation precision; i.e., sub-shot-noise sensing performance has been observed. Although schemes using quantum light emerge as a tool for ultimate sensing technology from diverse perspectives [27–29], sub-shot-noise quantum schemes for CD sensing have not yet been studied.

In this work, we identify and investigate optimal CD sensing schemes that exploit quantum states of light consistent with any given energy constraint. For generality, we allow for arbitrary ancilla-assisted sensing schemes where entanglement between the signal modes (i.e., LCP and RCP modes) and between the signal and ancillary modes can play a role. To assess the relative CD sensing performance of various schemes, we use quantum multiparameter estimation theory that gives a fundamental lower bound—namely, the quantum Cramér-Rao (QCR) bound—on the estimation uncertainty. The CD parameter is a function of two parameters that can vary independently. The estimation of such a global parameter can be classified into distributed sensing in a broad sense that a global parameter of interest is defined by multiple parameters given at different local modes, i.e., polarization modes in our work [30–32]. As explained in detail in Sec. II, this necessitates a multiparameter treatment of the problem even though only a single parameter is of eventual interest, as in a relative phase estimation in a Mach-Zehnder interferometer [33–35]. The QCR bound for CD sensing using any chosen probe is obtained using the quantum Fisher information matrix (QFIM) for a two-parameter problem, and limits the best precision achievable when the optimal quantum measurement is assumed to be used.

Using this approach, we first set the classical benchmark (CB) in CD sensing using a coherent state of light provided the optimal measurement is chosen. We then derive the ultimate quantum limit (UQL) by optimizing the QCR bound over all possible input probes, allowing for the probe-dependent optimal measurement in each case. It is shown that even in realistic situations with additional system loss, the UQL exhibits quantum enhancement in comparison with the CB. We then study measurements that can achieve the UQL for optimal probes. In particular, we show that the UQL can be achieved in an ancilla-free manner using Fock state probes with photon number resolving detection (PNRD). We show that using twin beams as an input can also achieve the UQL in an ancilla-assisted scheme, for which PNRD needs to be performed in both the signal and ancilla modes. Interestingly, the twin-beam input is shown to be advantageous even in a direct sensing scheme in which the twin beams interrogate the two polarization channels, and in which no ancilla modes are used. The latter scheme provides a practical setting that nearly achieves the UQL when losses are balanced at a moderate level and the difference in absorption between LCP and RCP modes is very small. Note that such a case applies to most CD sensing scenarios that study biochemical analytes [36], including DNA [37], hybrid nanostructures between nanocrystals and molecules [38], and biological

thiols [39]. In addition to the losses in the analyte which are being sensed, we explicitly take into account the effect of further system losses, e.g., those incurred in propagation and detection, making our results relevant to realistic laboratory implementations.

II. THEORETICAL MODELING

A. Circular dichroism sensing

Illuminating a chiral medium with either LCP or RCP light results in transmission (T), reflection (R), and absorption (A) into the individual polarization modes. The intensity ratios are denoted by T_{jk}, R_{jk}, and A_k for $j, k \in \{L, R\}$, with the constraint $\sum_j (T_{jk} + R_{jk}) + A_k = 1$, where the subscript $k(j)$ denotes the input (output) polarization. Apart from absorbance CD that can be quantified by the differential absorption, i.e., $A_L - A_R$, various alternative quantities can be measured to quantify the CD. A typical example would be transmission CD (TCD) defined as $T_{LL} - T_{RR}$ [40] or reflection CD defined as $R_{LL} - R_{RR}$ [41]. A polarization conversion in transmission or reflection may also occur, i.e., $T_{jk} \neq 0$ and $R_{jk} \neq 0$ for $j \neq k$, when the threefold rotational symmetry does not hold with respect to the direction of incidence [42]. The latter case causes circular conversion dichroism, i.e., $T_{LR} \neq T_{RL}$ [43].

In this work, not just for practical relevance with respect to realistic molecular samples or metamaterials that are typically considered, but also to eliminate the linear birefringence leading to unwanted polarization conversion, we focus on chiral media with a sufficiently large degree of rotational symmetry, for which $T_{jk} = 0$ for $j \neq k$ and $R_{jj} = 0$ for all j [44–47]. Indeed, for systems that are symmetric upon a discrete rotation of $2\pi/l$ with $l \geqslant 3$ along the optical axis, the lack of handedness-preserving reflection can be rigorously shown [48,49]. Furthermore, reciprocity imposes $R_{LR} = R_{RL}$ [8,50] for systems that are identical when seen from both sides; see, e.g., Refs. [8,50,51]. Under these conditions, the intensity difference of the transmitted LCP (I_L) and RCP (I_R) becomes the key quantity of interest to be measured in the usual CD measurement as illustrated in Fig. 1(a). Note that this is not an unduly restrictive assumption, and holds in the usual case in which chiral molecules in solution are randomly oriented relative to the incident field, and also for the vast majority of photonic materials designed for enhancing the CD signal. For the measurement outcomes to be obtained, we apply an appropriate estimator to estimate the quantity of TCD, defined as $\Gamma_- \equiv T_L - T_R$, where $T_j \equiv T_{jj}$.

For the quantum mechanical description of CD or TCD sensing, we consider an ancilla-assisted scheme as shown in Fig. 1(b). The annihilation operators $\hat{a}_L$ and $\hat{a}_R$ correspond to the LCP and RCP modes, respectively (the signal modes), whose state may be entangled with an arbitrary number of ancillary modes. Such a general setup allows us to consider entangled input states among the signal modes and ancilla modes or between the signal modes themselves. The transmission of each signal mode is described by a fictitious beam splitter with transmittance $T_{L(R)}$ while considering arbitrarily fixed phases that play no role in phase-insensitive detection which is normally employed in CD sensing [52]. An extra
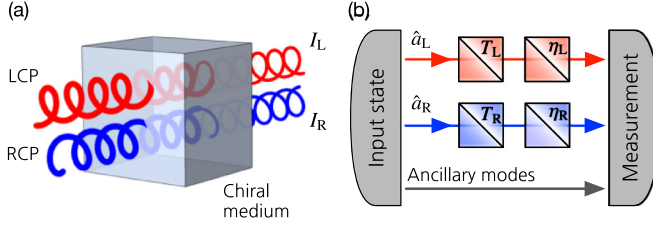
FIG. 1. (a) Traditional CD sensing: TCD is experimentally obtained by measuring the intensity difference of the transmitted LCP (I_L) and RCP (I_R) upon propagation through a chiral medium. (b) Quantum CD sensing: The ancilla-assisted CD sensing scheme is modeled quantum mechanically by the two signal modes corresponding to LCP and RCP and arbitrary ancillary modes that may be entangled with the signal modes. Beam splitters with transmittances $T_{L\,(R)}$ and $\eta_{L\,(R)}$ express two distinct processes in each mode: T_j expresses the transmittance of each polarization mode through the chiral medium, whereas η_j addresses extra loss of each mode such as nonunity channel transmission and detection efficiency of a detector.

loss that occurs outside the analyte (e.g., nonunity channel transmission or detection efficiency) is described by another fictitious beam splitter with transmittance $\eta_{L\,(R)}$ [53,54]. For calculation of the output state, the two consecutive beam splitters in the jth signal mode can be treated as a single beam splitter of transmittance $T_j\eta_j$. We assume, however, that the system has been well characterized in advance so that η_L and η_R are known. We also assume that the losses in the ancilla modes, which can be held in a controlled manner in many scenarios, are negligible. The associated input-output relation for the signal mode $j \in \{L, R\}$ is written as

$$\hat{a}_j \rightarrow \sqrt{T_j\eta_j}\,\hat{a}_j + \sqrt{\eta_j(1-T_j)}\,\hat{b}_j + \sqrt{(1-\eta_j)}\,\hat{c}_j, \quad (1)$$

where $\hat{b}_j$ and $\hat{c}_j$ are virtual input modes (their input states are assumed to be in the vacuum state) associated with the chiral medium and the system loss, respectively. It can be easily shown that the output operators satisfy the bosonic commutation relations $[\hat{a}_j, \hat{a}_k^\dagger] = \delta_{jk}$, implying that the effect of a vacuum noise is properly included through the lossy beam splitter model [55]. The input-output relation of Eq. (1) can thus be used to treat lossy problems. Also note that the above input-output relation describes the optical response of a single spectral mode under our assumption. Nevertheless, multiple spectral modes can also be treated by individual input-output relations with $T(\omega)$ and $\eta(\omega)$ that are generally frequency-dependent, when multimode quantum states of light need to be considered.

Equation (1) is applied to the two signal modes of the total input state $|\Psi_{in}\rangle$ containing ancillary modes. After tracing out the unobserved environment modes whose virtual initial states are assumed to be in a vacuum, the resultant output state $\hat{\rho}_{out}$ is measured using a chosen quantum measurement, yielding the outcomes $\boldsymbol{m}$. From these, the TCD parameter Γ_- is estimated. This is the general CD sensing scheme we aim to investigate in this work.

B. Quantum multiparameter estimation theory

The mean squared error or precision of CD sensing, a figure of merit which we consider in this work, can be

lower-bounded via quantum multiparameter estimation theory [56,57]. Consider an arbitrary pure state $|\Psi_{in}\rangle$ [58] as an input and suppose that the two transmittance parameters, $\boldsymbol{T} = (T_L, T_R)^T$, are estimated by means of an unbiased estimator $\check{\boldsymbol{T}}$ from the measurement results $\boldsymbol{m}$ that are drawn from a conditional probability distribution $p(\boldsymbol{m}|\boldsymbol{T})$. In this case, one can find that the 2×2 covariance matrix $\mathrm{Cov}(\check{\boldsymbol{T}}) = \langle(\check{\boldsymbol{T}} - \boldsymbol{T})(\check{\boldsymbol{T}} - \boldsymbol{T})^T\rangle$ obeys

$$\mathrm{Cov}(\check{\boldsymbol{T}}) \geqslant \frac{\boldsymbol{F}^{-1}}{\nu}, \quad (2)$$

where ν is the number of measurements being repeated and $\boldsymbol{F}$ is the Fisher information matrix (FIM) defined as [59,60]

$$\boldsymbol{F} = \begin{pmatrix} F_{LL} & F_{LR} \\ F_{RL} & F_{RR} \end{pmatrix}, \quad (3)$$

where the matrix elements are given by

$$F_{jk} = \sum_{\boldsymbol{m}} \frac{1}{p(\boldsymbol{m}|\boldsymbol{T})} \frac{\partial p(\boldsymbol{m}|\boldsymbol{T})}{\partial T_j} \frac{\partial p(\boldsymbol{m}|\boldsymbol{T})}{\partial T_k}, \quad (4)$$

where $j, k \in \{R, L\}$. The lower bound in Eq. (2) is called the Cramér-Rao (CR) bound and can always be saturated by a maximum-likelihood method in the limit of large ν [61,62].

The CR bound can potentially be further reduced via optimization of a measurement setting, leading to [59,60]

$$\mathrm{Cov}(\check{\boldsymbol{T}}) \geqslant \frac{\boldsymbol{F}^{-1}}{\nu} \geqslant \frac{\boldsymbol{H}^{-1}}{\nu}, \quad (5)$$

where $\boldsymbol{H}$ denotes the quantum Fisher information matrix (QFIM) defined by

$$H_{jk} = \mathrm{Tr}\left[\hat{\rho}_{\boldsymbol{T}} \frac{\hat{\mathcal{L}}_j \hat{\mathcal{L}}_k + \hat{\mathcal{L}}_k \hat{\mathcal{L}}_j}{2}\right], \quad (6)$$

with $\hat{\mathcal{L}}_j$ being a symmetric logarithmic derivative (SLD) operator associated with mode j [63]. It is a Hermitian solution of the equation

$$\frac{\partial \hat{\rho}_{\boldsymbol{T}}}{\partial T_j} = \frac{1}{2}(\hat{\rho}_{\boldsymbol{T}} \hat{\mathcal{L}}_j + \hat{\mathcal{L}}_j \hat{\rho}_{\boldsymbol{T}}) \quad (7)$$

for the parameter-encoded output state $\hat{\rho}_{\boldsymbol{T}}$. Here, $\boldsymbol{F}^{-1}$ and $\boldsymbol{H}^{-1}$ are understood as the inverse on their support if the matrices are singular, i.e., not invertible [64]. If the SLD operators $\hat{\mathcal{L}}_L$ and $\hat{\mathcal{L}}_R$ commute, the optimal measurement setting can be constructed over the common eigenbasis of the commuting SLD operators [65]; i.e., the lower bound in Eq. (5), called the QCR bound, can thus be said saturable in CD sensing [66].

Decomposing the state into the diagonalized bases, i.e., $\hat{\rho}_{\boldsymbol{T}} = \sum_n p_n |\psi_n\rangle\langle\psi_n|$ with $\langle\psi_n|\psi_m\rangle = \delta_{n,m}$, one can write the SLD operator as

$$\hat{\mathcal{L}}_j = \sum_n \frac{\partial_j p_n}{p_n} |\psi_n\rangle\langle\psi_n| + 2\sum_{n\neq m} \frac{p_n - p_m}{p_n + p_m} \langle\psi_m|\partial_j\psi_n\rangle |\psi_m\rangle\langle\psi_n|, \quad (8)$$

where summation runs over n, m for which $p_n + p_m \neq 0$ and $\partial_j \equiv \partial/\partial T_j$ for $j \in \{L, R\}$. Particularly when $|\partial_j\psi_n\rangle = 0$, the SLD operator $\hat{\mathcal{L}}_j$ of Eq. (8) becomes $\hat{\mathcal{L}}_j = \sum_n (p_n)^{-1}(\partial_j p_n)|\psi_n\rangle\langle\psi_n|$, for which the bases $\{|\psi_n\rangle\langle\psi_n|\}$ constitute the set of the optimal measurement bases [60].

Equation (5) is a matrix inequality: for two positive-semidefinite matrices $\boldsymbol{A}$ and $\boldsymbol{B}$, $\boldsymbol{A} \geqslant \boldsymbol{B}$ if and only if $\boldsymbol{A} - \boldsymbol{B}$ is a positive-semidefinite matrix. In other words, Eq. (5) means that

$$\boldsymbol{n}^{\mathrm{T}}\mathrm{Cov}(\check{\boldsymbol{T}})\boldsymbol{n} \geqslant \frac{\boldsymbol{n}^{\mathrm{T}}\boldsymbol{F}^{-1}\boldsymbol{n}}{\nu} \geqslant \frac{\boldsymbol{n}^{\mathrm{T}}\boldsymbol{H}^{-1}\boldsymbol{n}}{\nu}, \qquad (9)$$

for an arbitrary two-dimensional real vector $\boldsymbol{n}$ [67].

For CD sensing, $\Gamma_{-} = \boldsymbol{n}^{\mathrm{T}}\boldsymbol{T}$ with $\boldsymbol{n} = (1, -1)$. In this sense, CD sensing can be understood as an instance of distributed sensing, where one estimates a global parameter defined as a function of multiple local parameters associated with distinct quantum systems. Estimation of a global parameter $\Gamma = \sum_j n_j T_j$ defined as a linear combination of multiple local parameters has been much investigated for the case of unitary phase sensing [30–32,68,69]. Now, if $\check{\boldsymbol{T}}$ is an unbiased estimator of $\boldsymbol{T}$, $\check{\Gamma}_{-} = \check{T}_{\mathrm{L}} - \check{T}_{\mathrm{R}}$ is an unbiased estimator of Γ_{-}. Thus, it follows that

$$\mathrm{Var}(\check{\Gamma}_{-}) \equiv \boldsymbol{n}^{\mathrm{T}}\mathrm{Cov}(\check{\boldsymbol{T}})\boldsymbol{n} \geqslant \boldsymbol{n}^{\mathrm{T}}\boldsymbol{H}^{-1}\boldsymbol{n}, \qquad (10)$$

where the inequality follows from Eq. (9). Equation (10) is the sought QCR bound on the precision of CD sensing and is valid for any probe and any unbiased quantum measurement. Note that here, and in the sequel, we have dropped ν as it appears everywhere.

One may wonder whether multiparameter quantum estimation theory is really required for estimating the single parameter Γ_{-}. To appreciate the necessity of a multiparameter treatment, consider how a potential single-parameter treatment would proceed. One would first need to derive an SLD operator $\hat{\mathcal{L}}_{-}$ for Γ_{-} by solving the equation $\frac{\partial \hat{\rho}_{T}}{\partial \Gamma_{-}} = \frac{1}{2}(\hat{\rho}_{T}\hat{\mathcal{L}}_{-} + \hat{\mathcal{L}}_{-}\hat{\rho}_{T})$. However, the partial derivative on the left-hand side is ambiguous as it depends upon what variable—in general, some scalar function of $\boldsymbol{T}$ that uniquely determines it along with Γ_{-}—is held fixed while evaluating it. Different choices lead to different SLDs and different values for the QFIM. Unless one has additional information on $\boldsymbol{T}$ that indicates a choice of such a variable (e.g., if one knows that T_{R} is fixed at a given value), a multiparameter treatment is necessary. Since we do not assume any restrictions on how T_{L} and T_{R} vary, we must use a multiparameter treatment. This distinction between estimation of a scalar global parameter and single-parameter estimation is examined in detail in [32]. The same issue has already been intensively discussed in the case of estimating the relative phase between the arms of a Mach-Zehnder interferometer. It is well known that multiparameter estimation analysis is required to investigate the ultimate estimation bound of a single global parameter, which is the phase difference, when the two phases are unknown and not needed to be known individually [33–35].

In the next sections, we use the QCR bound to investigate the lower bounds to the estimation uncertainty or, equivalently, the precision of CD sensing for various input states of light. Individual cases are compared with the UQL which we shall derive below. One can see then what kinds of quantum states can achieve the UQL with and without assistance of ancillary modes. One of the main questions to be addressed using the multiparameter estimation approach is whether or not entangled states are necessary to achieve the UQL. Furthermore, the QCR bound is compared with the CR bound

calculated for a particular measurement and an input state we choose. The latter constitutes an explicit specification of the optimal measurement achieving the UQL.

III. QUANTUM CRAMÉR-RAO BOUND

A. Classical benchmark

To derive the optimal QCR bound when using classical light, let us consider first a product of coherent states as an input state in Fig. 1(b), i.e., $|\alpha_{\mathrm{L}}\rangle|\alpha_{\mathrm{R}}\rangle = \hat{D}_{\mathrm{L}}(\alpha_{\mathrm{L}})\hat{D}_{\mathrm{R}}(\alpha_{\mathrm{R}})|0\rangle|0\rangle$ in a direct sensing configuration. The coherent states are characterized by the average photon number $N_j = |\alpha_j|^2$ and the displacement operators are represented by $\hat{D}_j(\alpha_j) = \exp[\alpha\hat{a}_j^{\dagger} - \alpha^*\hat{a}_j]$. Applying the input-output relation of Eq. (1), the output state can be written as

$$|\Psi_{\mathrm{out}}\rangle_{\mathrm{coh}} = \left|\alpha_{\mathrm{L}}^{(\mathrm{out})}\right\rangle\left|\alpha_{\mathrm{R}}^{(\mathrm{out})}\right\rangle \qquad (11)$$

with $\alpha_j^{(\mathrm{out})} = \sqrt{\eta_j T_j}\alpha_j$. For such a pure output state, the QFIM of Eq. (6) can be calculated via [60,65,69]

$$H_{jk} = \frac{1}{2}\langle\Psi_{\mathrm{out}}|(\hat{\mathcal{L}}_j\hat{\mathcal{L}}_k + \hat{\mathcal{L}}_k\hat{\mathcal{L}}_j)|\Psi_{\mathrm{out}}\rangle, \qquad (12)$$

where the SLD operator $\hat{\mathcal{L}}_j$ can be written for a pure state $|\Psi_{\mathrm{out}}\rangle$ as

$$\hat{\mathcal{L}}_j = 2\partial_j(|\Psi_{\mathrm{out}}\rangle\langle\Psi_{\mathrm{out}}|). \qquad (13)$$

Through some algebraic calculation (see Appendix A for details), one can find that the QFIM for $\boldsymbol{T}$ with a coherent state input is diagonal and written as

$$\boldsymbol{H}_{\mathrm{coh}} = \mathrm{diag}\left(\frac{\eta_{\mathrm{L}}N_{\mathrm{L}}}{T_{\mathrm{L}}}, \frac{\eta_{\mathrm{R}}N_{\mathrm{R}}}{T_{\mathrm{R}}}\right). \qquad (14)$$

It is clear that $\boldsymbol{H}_{\mathrm{coh}} \to \boldsymbol{0}$ as $\eta_{\mathrm{L/R}} \to 0$. By substituting $\boldsymbol{H}_{\mathrm{coh}}$ to Eq. (10), the QCR bound to the estimation uncertainty of Γ_{-} can thus be written as

$$\mathrm{Var}(\check{\Gamma}_{-})_{\mathrm{coh}} = \frac{T_{\mathrm{L}}}{\eta_{\mathrm{L}}N_{\mathrm{L}}} + \frac{T_{\mathrm{R}}}{\eta_{\mathrm{R}}N_{\mathrm{R}}}. \qquad (15)$$

Defining the ratio $r = N_{\mathrm{L}}/N_{\mathrm{tot}}$ for the total average intensity in the signal modes $N_{\mathrm{tot}} = N_{\mathrm{L}} + N_{\mathrm{R}}$, which we fix throughout this work as a constraint, we find that the optimal ratio can be written as

$$r_{\mathrm{opt}} = \frac{1}{1 + \sqrt{\frac{\eta_{\mathrm{L}}T_{\mathrm{R}}}{\eta_{\mathrm{R}}T_{\mathrm{L}}}}}, \qquad (16)$$

for which the QCR bound of Eq. (15) is minimized and thus reads

$$\mathrm{Var}(\check{\Gamma}_{-})_{\mathrm{coh}}^{\mathrm{opt}} = \frac{1}{N_{\mathrm{tot}}}\left(\sqrt{\frac{T_{\mathrm{L}}}{\eta_{\mathrm{L}}}} + \sqrt{\frac{T_{\mathrm{R}}}{\eta_{\mathrm{R}}}}\right)^2. \qquad (17)$$

The optimal ratio r_{opt} of Eq. (16) is presented in Fig. 2(a) as a function of $\eta_{\mathrm{L}}T_{\mathrm{R}}/\eta_{\mathrm{R}}T_{\mathrm{L}}$ in log scale, while shown in Fig. 2(b) as a function of T_{L} and T_{R} in log scale for balanced losses, i.e., $\eta_{\mathrm{L}} = \eta_{\mathrm{R}}$. They clearly show that more energy needs to be injected into a more lossy signal mode to keep the optimal intensity balance between the signal modes, written as

$$N_{\mathrm{L}} : N_{\mathrm{R}} = \sqrt{\frac{T_{\mathrm{L}}}{\eta_{\mathrm{L}}}} : \sqrt{\frac{T_{\mathrm{R}}}{\eta_{\mathrm{R}}}}. \qquad (18)$$
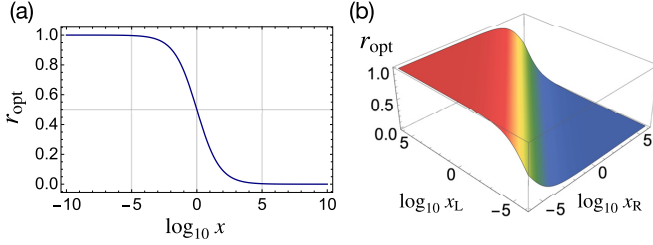
FIG. 2. (a) The optimal ratio r_{opt} as a function of logarithmic $x = \eta_L T_R / \eta_R T_L$ for a coherent state input. The x is replaced by $x = \eta_L T_R (1 - \eta_R T_R) / \eta_R T_L (1 - \eta_L T_L)$ for the optimal state input achieving the UQL to the precision of CD sensing. (b) The optimal ratio r_{opt} is shown as a function of logarithmic $x_L = T_L$ and $x_R = T_R$ for a coherent state input when $\eta_L = \eta_R$. The axis labels are transformed to $x_L = T_L (1 - \eta_L T_L)$ and $x_R = T_R (1 - \eta_R T_R)$ for the optimal state input.

In most cases, the difference in transmission between LCP and RCP light is extremely small and in good approximation it can be assumed that they are close to equal, i.e., $T_j = T_k$. Provided losses are balanced $\eta_j = \eta_k$, the same amount of energies, i.e., $N_L = N_R$, would be, to a very good approximation, the optimal choice in a classical sensing scheme, for which $\text{Var}(\check{\Gamma}_-)^{opt}_{coh} = 4T / \eta N_{tot}$ with $T \equiv T_{L/R}$ and $\eta \equiv \eta_{L/R}$. In cases where the two transmittances cannot be assumed to be equal, our findings can be combined with an adaptive scheme [70,71]. There, the input energies between LCP and RCP modes are adjusted (e.g., using a Bayesian approach) in real time, based on prior information about the parameter being updated over repetition of the measurement.

A general classical state of light in an ancilla-assisted configuration can be written as a mixture of product coherent states as follows:

$$\hat{\rho}_{coh} = \int p(\alpha_L, \alpha_R, \alpha_A) |\alpha_L, \alpha_R, \alpha_A\rangle \langle \alpha_L, \alpha_R, \alpha_A | d\alpha_L d\alpha_R d\alpha_A, \tag{19}$$

with $\text{Tr}[\hat{a}_j^\dagger \hat{a}_j \hat{\rho}_{coh}] = N_j$. Applying the convexity of the QFIM [35], one can prove that the QCR bound to be obtained for the input of Eq. (19) is always equal to or greater than the CB of Eq. (17). Therefore, neither ancillary modes nor classical correlation are useful.

B. Ultimate quantum limit

Let us now derive the UQL on the estimation uncertainty of the TCD parameter Γ_-. When $\eta_{L/R} = 1$, the maximum QFIM (in the matrix inequality sense) for two intensity parameters (T_L, T_R), optimized over all input states, has been found in Ref. [72] and can be written as

$$H_{max}^{lossless} = \text{diag}\left(\frac{N_L}{T_L(1 - T_L)}, \frac{N_R}{T_R(1 - T_R)} \right). \tag{20}$$

The QCR inequality (9) associated with $H_{max}^{lossless}$ is then the lowest possible for the given energy constraints since $A \geqslant B$ implies $A^{-1} \leqslant B^{-1}$ for any two positive-definite matrices A and B. It was also shown in [72] that it can be achieved in general by so-called number-diagonal signal probes in an ancilla-assisted scheme and in particular by a pair of Fock

state inputs without ancilla modes when N_L and N_R are integers [73].

In the presence of excess loss (i.e., $\eta_{L/R} \neq 1$), the SLD operators $\hat{\mathcal{L}}_j$, the lossless case leading to Eq. (20), are modified to $\hat{\mathcal{S}}_j$, given by (see Appendix B for details)

$$\hat{\mathcal{S}}_j = \eta_j \hat{\mathcal{L}}_j, \tag{21}$$

for $j \in \{L, R\}$. This leads to $H_{max}^{lossless}$ of Eq. (20) being replaced by

$$H_{max} = \text{diag}\left(\frac{\eta_L N_L}{T_L(1 - \eta_L T_L)}, \frac{\eta_R N_R}{T_R(1 - \eta_R T_R)} \right). \tag{22}$$

This is the maximum QFIM for two transmittance parameters (T_L, T_R) in the presence of additional loss. It is clear that $H_{max} \to 0$ as $\eta_{L/R} \to 0$. Note that if correlated probes are used, the QFIM is not diagonal in general, but the above result shows that the maximum QFIM of Eq. (22) is diagonal, meaning that it can be obtained by independent quantum probes. In particular, no choice of probe state can yield a lower variance in estimating T_L or T_R.

The UQL to the uncertainty $\text{Var}(\check{\Gamma}_-)$ of the CD parameter can now be readily obtained using Eq. (10):

$$\text{Var}(\check{\Gamma}_-)_{UQL} = \frac{T_L(1 - \eta_L T_L)}{\eta_L N_L} + \frac{T_R(1 - \eta_R T_R)}{\eta_R N_R}. \tag{23}$$

This is the UQL to the estimation uncertainty of CD sensing for optimal probes with arbitrarily given N_L and N_R.

One can easily show that the optimal ratio r_{opt} that minimizes $\text{Var}(\check{\Gamma}_-)_{UQL}$ of Eq. (23) can be written as

$$r_{opt} = \frac{1}{1 + \sqrt{\frac{\eta_L T_R (1 - \eta_R T_R)}{\eta_R T_L (1 - \eta_L T_L)}}}, \tag{24}$$

for which

$$\text{Var}(\check{\Gamma}_-)_{UQL}^{opt} = \frac{1}{N_{tot}} \left(\sqrt{\frac{T_L(1 - \eta_L T_L)}{\eta_L}} + \sqrt{\frac{T_R(1 - \eta_R T_R)}{\eta_R}} \right)^2. \tag{25}$$

This is the UQL to the precision of CD sensing and is obtained when optimal probes whose signal modes satisfying the optimal intensity ratio of Eq. (24) between N_L and N_R are measured by the optimal measurement setting. The UQL applies to both cases with and without ancillary modes. Furthermore, the optimal schemes for scenarios without excess loss found in Ref. [72] can be used to reach the UQL of Eq. (25) in lossy scenarios.

Comparing the UQL of Eq. (25) with the CB of Eq. (17), one can see that the quantum enhancement is achieved by the factors of $(1 - \eta_L T_L)$ and $(1 - \eta_R T_R)$ in the numerator of the respective terms, but diminishes with loss, i.e., as $\eta_{L/R} \to 0$. Note that both QCR bounds of Eqs. (17) and (25) scale with N_{tot}, i.e., following the shot-noise scaling in terms of the total energy N_{tot}, as in the single loss parameter estimation case [73]. The optimal ratio r_{opt} of Eq. (24) exhibits the same behavior as shown in Figs. 2(a) and 2(b), but with $\eta_L T_R (1 - \eta_R T_R) / \eta_R T_L (1 - \eta_L T_L)$ and $x_j = T_j(1 - \eta_j T_j)$ for $j = L, R$, respectively. The optimal ratio r_{opt} can also be understood as the optimal balance of the average intensities between the
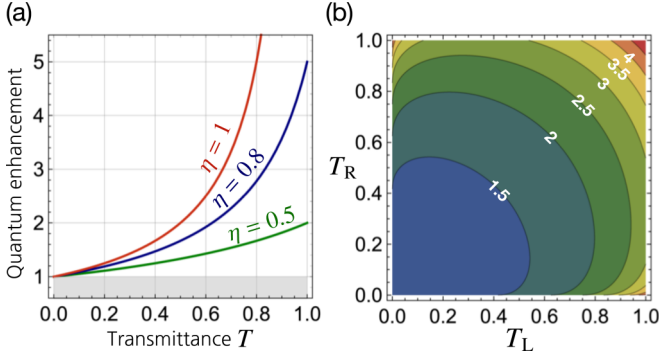
FIG. 3. (a) Quantum enhancement $\text{Var}(\check{\Gamma}_-)_{\text{CB}}/\text{Var}(\check{\Gamma}_-)_{\text{UQL}}$ in terms of transmittance T for $\eta = 1, 0.8, 0.5$ when $T_{\text{L/R}} = T$ and $\eta_{L/R} = \eta$ can be assumed. (b) Quantum enhancement $\text{Var}(\check{\Gamma}_-)_{\text{CB}}/\text{Var}(\check{\Gamma}_-)_{\text{UQL}}$ in terms of T_{L} and T_{R} for $\eta = 0.8$.

LCP and RCP modes, written as

$$N_{\text{L}} : N_{\text{R}} = \sqrt{\frac{T_{\text{L}}(1 - \eta_{\text{L}} T_{\text{L}})}{\eta_{\text{L}}}} : \sqrt{\frac{T_{\text{R}}(1 - \eta_{\text{R}} T_{\text{R}})}{\eta_{\text{R}}}}. \quad (26)$$

Again, in most cases, $T_j \approx T_k$ and $\eta_j \approx \eta_k$, so the same amount of energies, i.e., $N_{\text{L}} = N_{\text{R}}$, would be the optimal choice in the ultimate CD sensing scheme, for which $\text{Var}(\check{\Gamma}_-)_{\text{UQL}}^{\text{opt}} = 4T(1 - \eta T)/\eta N_{\text{tot}}$ with $T \equiv T_{\text{L/R}}$ and $\eta \equiv \eta_{\text{L/R}}$. In this case, the quantum enhancement of the UQL as compared to the CB can be quantified by the ratio defined as

$$\frac{\text{Var}(\check{\Gamma}_-)_{\text{coh}}^{\text{opt}}}{\text{Var}(\check{\Gamma}_-)_{\text{UQL}}^{\text{opt}}} = \frac{1}{1 - \eta T}. \quad (27)$$

Note that this enhancement factor diverges as $\eta T \to 1$, so the infinite-fold enhancement can be in principle achieved or a huge quantum enhancement can be exploited in well-controlled situations. The enhancement is degraded as η decreases in lossy cases; e.g., the maximal enhancement is only twofold for $\eta = 0.5$. The enhancement factor is presented in Fig. 3(a) as a function of transmittance T for $\eta = 1, 0.8$, and 0.5. It clearly shows that the quantum enhancement is sensitive to the loss parameter η, so reducing the loss in a sensing setup is crucial to increase the quantum enhancement for a given $T_{\text{L}} \approx T_{\text{R}} = T$ in CD sensing. We, nevertheless, stress that the quantum enhancement factor is always greater than unity unless either η or T is zero. Figure 3(b) shows an overall quantum enhancement in terms of arbitrary T_{L} and T_{R} for balanced loss $\eta = 0.8$ chosen as an example.

C. Fock state input

We now show that the Fock state input $|N_{\text{L}}\rangle|N_{\text{R}}\rangle$ without using ancillary modes can achieve the UQL. Through the beam splitter transformation of Eq. (1), the output state can be written as

$$\hat{\rho}_{\text{Fock}} = \sum_{m_{\text{L}}, m_{\text{R}}} p(m_{\text{L}}, m_{\text{R}}|\boldsymbol{T}) |m_{\text{L}}, m_{\text{R}}\rangle \langle m_{\text{L}}, m_{\text{R}}|, \quad (28)$$

where

$$p(m_{\text{L}}, m_{\text{R}}|\boldsymbol{T}) = \prod_{j=\text{L,R}} \binom{N_j}{m_j} (\eta_j T_j)^{m_j} (1 - \eta_j T_j)^{N_j - m_j}. \quad (29)$$

With this, one can show that the QFIM is equal to $\boldsymbol{H}_{\text{max}}$ of Eq. (22), finally achieving the UQL of Eq. (25) when the photon numbers N_{L} and N_{R} follow the optimal ratio of Eq. (26). We omit the detailed calculation here, since we explicitly write down in Sec. IV B an estimator $\check{\Gamma}_-$ that achieves the UQL. Therefore, Fock state input $|N_{\text{L}}\rangle|N_{\text{R}}\rangle$ is an optimal probe to reach the UQL to the precision in CD sensing. This shows that the UQL in CD sensing can be achieved without entanglement.

The UQL is inversely proportional to the total average photon number N_{tot}, so it is recommended to increase the total intensity of an input state while keeping the optimal ratio of Eq. (26). However, large Fock states with $N_j \gg 1$ cannot be readily generated with current technology [74–76]. As shown in Ref. [72], an alternative way is to use N_j single-photon probes [77–79], which also leads to the UQL on the precision of CD sensing.

D. Twin-beam input

Another useful quantum source of light is the so-called twin beam. These have widely been used in many applications including quantum imaging [80], quantum illumination [81–84], and quantum sensing [85] due to the strong photon number correlation [86–89]. The twin-beam state can be generated from a spontaneous parametric down-conversion process [90–92] and is formally written as the two-mode squeezed vacuum (TMSV) state, $|\text{TMSV}\rangle = \hat{S}_2(\xi)|00\rangle$ with the two-mode squeezing operator $\hat{S}_2(\xi) = \exp[\xi^* \hat{a}\hat{b} - \xi \hat{a}^\dagger \hat{b}^\dagger]$ for $\xi = re^{i\theta}$ with $\{r, \theta\} \in \mathbb{R}$. As shown below, such TMSV states or twin beams can be used for CD sensing in two ways.

First, let us consider a CD sensing scheme using two TMSV states $|\text{TMSV}\rangle \otimes |\text{TMSV}\rangle$ in an ancilla-assisted configuration. Let us assume that the respective signal modes of the TMSV states are sent to LCP and RCP mode, while their respective ancillary modes are held losslessly. Such a setting has been shown to achieve the QFIM of Eq. (20) for $(T_{\text{L}}, T_{\text{R}})$ in the absence of additional loss [72]. It is known that when estimating a single net transmittance parameter τ, the estimation uncertainty $\Delta\tau^2 = \tau(1 - \tau)/N$ can be achieved by a TMSV state in an ancilla-assisted configuration [72]. This can be extended to the estimation of two parameters τ_{L} and τ_{R}; using TMSV states separately for each parameter estimation can achieve the estimation uncertainties written as $\tau_{\text{L}}(1 - \tau_{\text{L}})/N_{\text{L}}$ and $\tau_{\text{R}}(1 - \tau_{\text{R}})/N_{\text{R}}$, respectively. Here, the τ's denote the net transmittance that includes both the transmittance of a sample under investigation and a system loss, i.e., $\tau_{\text{L}} = T_{\text{L}}\eta_{\text{L}}$ and $\tau_{\text{R}} = T_{\text{R}}\eta_{\text{R}}$. Rescaling the estimators $\hat{\tau}_{\text{L}}$ and $\hat{\tau}_{\text{R}}$ of τ_{L} and τ_{R} respectively by their respective losses $1/\eta_{\text{L}}$ and $1/\eta_{\text{R}}$ and subtracting them gives an estimate of $\Gamma_- = T_{\text{L}} - T_{\text{R}}$ with the estimation uncertainty equal to the UQL of Eq. (25); the variances originating from independent TMSV states are simply added. This proves the optimality of the scheme. Furthermore, note that the correlation between the input photon number in the signal and ancilla mode plays an important role in that a photon number measurement on the ancilla mode gives information on the photon number on the signal mode. It consequently reduces the estimation uncertainty. The analysis in Sec. III B also implies that the same setting can be used to achieve the UQL of Eq. (25) when the average

intensities of the signal states of the two TMSV states satisfy the optimal ratio of Eq. (26). Therefore, the twin-beam input is another optimal state that reaches the UQL to the precision in CD sensing in an ancilla-assisted configuration. One can find other optimal states in the ancilla-assisted scheme according to the analysis in Ref. [72].

A second way to use the TMSV state input is to inject the two modes of a single TMSV state into LCP and RCP modes, respectively. Note that ancillary modes are not considered in such direct sensing scheme and $N_L = N_R = \sinh^2 r \equiv N$ as an intrinsic feature of the twin-beam state. The output state $\hat{\rho}_T$ can be obtained by using the input-output relation of Eq. (1) for the input state $|\text{TMSV}\rangle$. In this particular case, analytical calculation of the QFIM using SLD operators is tricky, so we use the quantum fidelity of Eq. (C3) that can be calculated more easily using a closed expression [93,94]. Leaving all the technical details to Appendix C, we finally have the QFIM written as

$$H_{jj} = \frac{\chi_{j\bar{j}}\eta_j N}{T_j(1 - \eta_j T_j)},\tag{30}$$

$$H_{jk} = \frac{-\eta_j\eta_k N(N+1)}{1 + \eta_j T_j(1 - \eta_k T_k)N + \eta_k T_k(1 - \eta_j T_j)N},\tag{31}$$

with

$$\chi_{j\bar{j}} = \frac{1 - \eta_j T_j(1 - \eta_{\bar{j}}T_{\bar{j}}) + \eta_{\bar{j}}T_{\bar{j}}(1 - \eta_j T_j)N}{1 + \eta_j T_j(1 - \eta_{\bar{j}}T_{\bar{j}})N + \eta_{\bar{j}}T_{\bar{j}}(1 - \eta_j T_j)N},\tag{32}$$

where $j \neq k \in \{L, R\}$, $\bar{j} = R$ if $j = L$, and vice versa.

In comparison with the QFIM of Eq. (22), the diagonal element H_{jj} of Eq. (30) contains the additional factor χ_{jk} coming from the correlation between the signal modes. One can show that $0 \leqslant \chi_{jk} \leqslant 1$ holds, where the upper bound is reached when $\eta_j T_j = 0$ or $\eta_k T_k = 1$, while the lower bound is obtained when $\eta_j T_j = 1$ and $\eta_k T_k = 0$. The QCR bound for the estimation uncertainty $\text{Var}(\check{\Gamma}_-)$ can thus be written in terms of Eqs. (30) and (31) as

$$\text{Var}(\check{\Gamma}_-)_{\text{TMSV}} = \frac{H_{LL} + H_{RR} + H_{LR} + H_{RL}}{H_{LL}H_{RR} - H_{LR}H_{RL}}.\tag{33}$$

It can be easily shown that the use of a TMSV state input in a direct sensing scheme cannot achieve the UQL to the precision of CD sensing. However, one can find that the QCR bound $\text{Var}(\check{\Gamma}_-)_{\text{TMSV}}$ of Eq. (33) becomes similar to the UQL at some regimes of parameters, which we elaborate on in more detail below.

For comparison of $\text{Var}(\check{\Gamma}_-)_{\text{TMSV}}$ with the other cases, let us set $N_{\text{tot}} = 2N = 2$ and $\eta_L = \eta_R = 0.8$ as an example without loss of generality. In Fig. 4(a), we show that the quantum enhancement $\text{Var}(\check{\Gamma}_-)_{\text{coh}}^{\text{opt}}/\text{Var}(\check{\Gamma}_-)_{\text{TMSV}}$ is limited to only the presented region. Such a beneficial region depends on the values of N and $\eta_{L(R)}$, but in a particular region of interest for CD sensing; i.e., when $T_L \approx T_R$, the enhancement is always present and significant. More interestingly and clearly, it can be shown that $\text{Var}(\check{\Gamma}_-)_{\text{TMSV}} = \text{Var}(\check{\Gamma}_-)_{\text{UQL}}^{\text{opt}}$ holds up to the first order in δT for $T_R = T_L + \delta T$ when losses are equally balanced $\eta_L = \eta_R$. Such a feature is evident in Figs. 4(a) and 4(b) around the region where $T_L \approx T_R$. This indicates that in most cases when T_L and T_R can be assumed in good approximation as equal, one can use the direct sensing scheme with
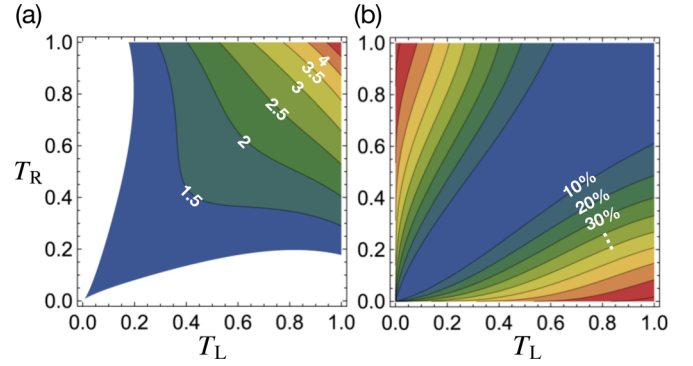

FIG. 4. (a) Quantum enhancement $\text{Var}(\check{\Gamma})_{\text{CB}}/\text{Var}(\check{\Gamma}_-)_{\text{TMSV}}$ in terms of T_L and T_R for balanced losses $\eta = 0.8$. (b) The normalized difference between $\text{Var}(\check{\Gamma}_-)_{\text{TMSV}}$ and $\text{Var}(\check{\Gamma}_-)_{\text{UQL}}^{\text{opt}}$ for $\eta = 0.8$. Here, $N_{\text{tot}} = 2$ is assumed as an example.

the TMSV state input as a practical scheme. The use of TMSV state input also promises quantum enhancement for any value of $T \equiv T_L = T_R$, as already shown in Fig. 3. This is an important finding as it opens a practical path toward exploiting of practical quantum resources in realistic CD sensing.

It is worth discussing the role of the average photon number N in $\text{Var}(\check{\Gamma}_-)_{\text{TMSV}}$. A noticeable behavior is revealed in the limit of large N. Both $\text{Var}(\check{\Gamma}_-)_{\text{UQL}}^{\text{opt}}$ and $\text{Var}(\check{\Gamma}_-)_{\text{coh}}^{\text{opt}}$ approach zero as $N \to \infty$, whereas $\text{Var}(\check{\Gamma}_-)_{\text{TMSV}}$ becomes

$$\text{Var}(\check{\Gamma}_-)_{\text{TMSV}}|_{N \to \infty}$$
$$= \frac{(T_L - T_R)^2(1 - \eta_L T_L)(1 - \eta_R T_R)}{1 + \eta_L T_L(1 - \eta_R T_R) + \eta_R T_R(1 - \eta_L T_L)}.\tag{34}$$

This implies that the use of the TMSV state input outperforms the CB only when $T_L \approx T_R$ or N is small. In other words, as N is reduced, the beneficial region in Fig. 4(c) becomes wider, but never covers the entire region. This means that no quantum enhancement is obtained in direct sensing with a twin beam when either T_L or T_R is too small even in the limit $N \to 0$. Such a region is of course not of much interest for CD sensing, but could be significant for other applications.

E. Signal-to-noise ratio

For an estimator $\check{\Gamma}_-$, one can define the signal-to-noise ratio of an estimate of Γ_- as

$$\text{SNR} = \frac{\langle\check{\Gamma}_-\rangle^2}{\text{Var}(\check{\Gamma}_-)},\tag{35}$$

where $\langle\check{\Gamma}_-\rangle^2 = \Gamma_-^2$ for an unbiased estimator. Using Eq. (9), one can easily show that for a given input state the SNR is upper bounded as

$$\text{SNR} \leqslant \frac{\Gamma_-^2}{\text{Var}(\check{\Gamma}_-)_{\text{QCR}}},\tag{36}$$

where $\text{Var}(\check{\Gamma}_-)_{\text{QCR}}$ is the QCR bound to $\text{Var}(\check{\Gamma}_-)$. This shows that the upper bound of SNR becomes higher by increasing Γ_- while decreasing $\text{Var}(\check{\Gamma}_-)_{\text{QCR}}$. In other words, precise sensing with small $\text{Var}(\check{\Gamma}_-)_{\text{QCR}}$ yields high SNR, but its inverse does not hold. This implies that assessment of CD sensing in terms of SNR does not guarantee precise estimation of CD or TCD

parameter. The inequality in Eq. (36) can be saturated when the optimal measurement setting and the optimal estimator are used for a given state. A similar SNR inequality for a single-parameter estimation has also been discussed in Ref. [60].

IV. MEASUREMENTS ACHIEVING THE ULTIMATE QUANTUM LIMIT

Let us now consider particular measurement settings to examine whether the CR bound reaches the QCR bound for individual cases. In this work we employ direct-detection measurements at each output port in Fig. 1(b), which measures the intensities of the transmitted signal modes through a chiral medium and ancillary modes having been kept unaltered. In particular, a PNRD yields the multidimensional photon number distribution for the measurement outcomes $\boldsymbol{m}$ drawn from the underlying conditional probability $p(\boldsymbol{m}|\boldsymbol{T})$, using which the CR bound can be evaluated. In terms of concrete estimators, it may be expected that the scaled sample mean for the photon numbers detected in the individual output is an efficient estimator of Γ_- [62,95]. As we show below, this is true even for a finite sample size in many cases.

A. Coherent state input

For a coherent state input in a direct sensing configuration, the output state is given as Eq. (11) and the probability distribution of detecting $m_{\rm L}$ and $m_{\rm R}$ photons at the respective output ports is written as

$$p(m_{\rm L}, m_{\rm R}|\boldsymbol{T}) = \prod_{j={\rm L,R}} e^{-\eta_j T_j N_j} \frac{(\eta_j T_j N_j)^{m_j}}{m_j!}. \quad (37)$$

Using Eq. (4), one can show that the FIM with Eq. (37) is the same as QFIM of Eq. (14), implying that the PNRD is the optimal measurement setting to reach the optimal classical bound of Eq. (15) when $N_{\rm L}$ and $N_{\rm R}$ are arbitrarily chosen or the CB of Eq. (17) when the optimal ratio between $N_{\rm L}$ and $N_{\rm R}$ is chosen.

Furthermore, the estimator

$$\check{\Gamma}_- := \frac{m_{\rm L}}{\eta_{\rm L} N_{\rm L}} - \frac{m_{\rm R}}{\eta_{\rm R} N_{\rm R}} \quad (38)$$

of Γ_- is clearly unbiased. Based on the independent Poisson distributions (37) of $m_{\rm L}$ and $m_{\rm R}$, we have that $\mathrm{Var}(\check{\Gamma}_-) = \frac{T_{\rm L}}{\eta_{\rm L} N_{\rm L}} + \frac{T_{\rm R}}{\eta_{\rm R} N_{\rm R}}$, which is identical to the QFIM-based limit of Eq. (15). This estimator is therefore quantum-optimal even on a single-shot basis.

B. Fock state input

For a Fock state input without ancillary modes, the output state of Eq. (28) is diagonalized over the photon number states $\{|m_{\rm L}, m_{\rm R}\rangle\}$. It is clear that the diagonalized basis is independent of the parameter $\boldsymbol{T}$, so the second term in Eq. (8) vanishes and consequently the FIM of Eq. (4) is the same as the QFIM of Eq. (22). This indicates that the PNRD offers an optimal measurement setting for Fock state probes. The optimality of the PNRD can also be proved from the fact that the eigenstates of the corresponding SLD operator are the photon number states $\{|m_{\rm L}, m_{\rm L}\rangle\}$ [60,96].

Consider again the estimator of Eq. (38) based on a linear combination of the counting measurements. $m_{\rm L}$ and $m_{\rm R}$ have binomial distributions $\mathrm{Bin}(N_{\rm L}, \eta_{\rm L} T_{\rm L})$ and $\mathrm{Bin}(N_{\rm R}, \eta_{\rm R} T_{\rm R})$ with means $\eta_{\rm L} T_{\rm L} N_{\rm L}$ and $\eta_{\rm R} T_{\rm R} N_{\rm R}$ and variances $\eta_{\rm L} T_{\rm L} N_{\rm L}(1 - \eta_{\rm L} T_{\rm L})$ and $\eta_{\rm R} T_{\rm R} N_{\rm R}(1 - \eta_{\rm R} T_{\rm R})$, respectively. It follows that $\check{\Gamma}_-$ is an unbiased estimator of Γ_- and has the variance

$$\mathrm{Var}(\check{\Gamma}_-) = \frac{T_{\rm L}(1 - \eta_{\rm L} T_{\rm L})}{\eta_{\rm L} N_{\rm L}} + \frac{T_{\rm R}(1 - \eta_{\rm R} T_{\rm R})}{\eta_{\rm R} N_{\rm R}}, \quad (39)$$

which agrees with the UQL of Eq. (23). The estimator $\check{\Gamma}_-$ is thus a quantum-optimal estimator even on a single-shot basis.

Similar considerations show that the scaled sample mean of the photon counts achieves the UQL even when multiple Fock states are used in succession to probe the sample. If multiple single photons are used [77–79] instead of large Fock states that are yet unavailable with current technology, we can additionally relax the requirement of using PNRDs and use single-photon detectors instead, which are a well-established technology [97].

C. Twin-beam input

When using twin beams in the ancilla-assisted configuration, the QFIM of Eq. (20) has been shown to be achievable by performing PNRD in all four modes, i.e., two signal and two ancillary modes [72]. As explained in Sec. III B, such optimality of the measurement scheme also carries over to the measurement of CD in the presence of loss, consequently achieving the UQL. The maximum-likelihood estimator then provides an efficient estimator of Γ_-, at least in the limit of a large number of copies [62,95].

As a practical matter, we mention that to reach the same bound, one can use $M = N/n$ copies of weakly squeezed TMSVs with the average photon number of $n \ll 1$ on each mode and perform direct detection on each two-mode output state [72]. Apart from placing fewer demands on high squeezing required in the twin beam, weak fields with $n \ll 1$ allow us to perform, instead of PNRD, single-photon detection [97].

For a direct sensing scheme with a TMSV state input, the output state is a mixed state and not diagonalized over the photon number states. The photon number distribution of the output state is given as

$$p(m_{\rm L}, m_{\rm R}|\boldsymbol{T}) = \sum_{n=0}^{\infty} \frac{N^n}{(N+1)^{n+1}} \prod_{j={\rm L,R}} f_j(n), \quad (40)$$

where $f_j(n) = \binom{n}{m_j}(\eta_j T_j)^{m_j}(1 - \eta_j T_j)^{n-m_j}$. In this case, we numerically calculate the $\boldsymbol{F}$ of Eq. (4), which gives rise to the CR bound. The latter is compared with the QCR bound $\mathrm{Var}(\check{\Gamma}_-)_{\rm TMSV}$ and the UQL $\mathrm{Var}(\check{\Gamma}_-)_{\rm UQL}$ for balanced losses $\eta = 0.8$ chosen as an example. They are shown in Figs. 5(a) and 5(b), respectively. The CR bound is not generally the same as the QCR bound $\mathrm{Var}(\check{\Gamma}_-)_{\rm TMSV}$, but they become extremely similar when $T_{\rm L}$ and $T_{\rm R}$ are close to each other, as shown in Fig. 5(a). This indicates that the CR bound can also be similar the UQL $\mathrm{Var}(\check{\Gamma}_-)_{\rm UQL}$ in the region where $T_{\rm L} \approx T_{\rm R}$. The latter behavior is evident in Fig. 5(b). Especially, one can show that the CR bound becomes exactly the same as the other two bounds when $T_{\rm L} = T_{\rm R}$. This means that one can
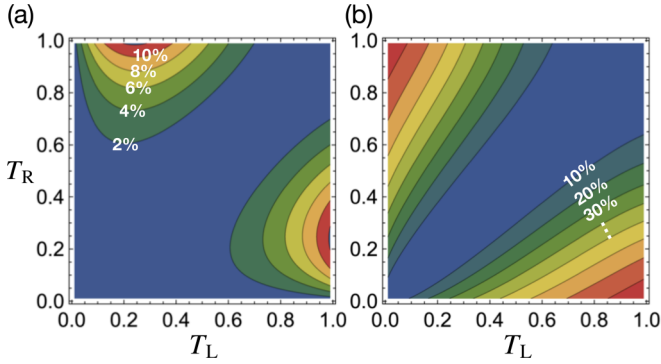
FIG. 5. (a) The normalized difference between the CR bound for PNRD and the QCR bound $\mathrm{Var}(\check{\Gamma}_-)_{\mathrm{TMSV}}$ for balanced losses $\eta = 0.8$. (b) The normalized difference between the CR bound for PNRD and the UQL $\mathrm{Var}(\check{\Gamma}_-)_{\mathrm{UQL}}^{\mathrm{opt}}$ for $\eta = 0.8$. Here, $N_{\mathrm{tot}} = 2$ is assumed as an example.

use the direct sensing scheme with the twin-beam state input and PNRD as a practically optimal scheme for CD sensing when $T_{\mathrm{L}} \approx T_{\mathrm{R}}$ can be assumed and losses are balanced. In this case, a quantum enhancement comes from the strong photon number correlation shared between the two modes in the twin-beam state.

V. CONCLUSION

Through multiparameter estimation theory applied for a single global parameter $\Gamma_- = T_{\mathrm{L}} - T_{\mathrm{R}}$, we have obtained the UQL (i.e., ultimate quantum limit) on the precision of CD (i.e., circular dichroism) sensing and identified the optimal CD sensing schemes to achieve it. With the optimal schemes (using either separable or entangled probe states) studied in this work, a significant quantum enhancement has been shown to be achievable even in the presence of additional system loss. For most samples of chiral media being analyzed by CD measurement, the difference between the transmittance parameters T_{L} and T_{R} is very small. For such usual cases, we have proposed a practical CD sensing scheme to reach nearly the UQL, which requires only to use the twin-beam state as an input and to perform PNRD (i.e., photon-number-resolving detection) at the two signal modes. Since the latter scheme only uses feasible technologies [98–100], which have widely been used in quantum optics for the last few decades, we expect our theoretical work to motivate more diverse studies in various chirality sensing. We further believe that the results shown here will be useful in a wide variety of scientific domains such as chemistry, biology, nanophotonics, quantum information science, and quantum metrology.

The results shown in this work indicate that practical enhancement of CD sensing with quantum light has no fundamental obstacles. We mention, however, that generating nonclassical states at desired frequencies at which CD occurs is vital to see a quantum enhancement [101,102]. In complex systems, although less common, when the analysis of the CD signal requires measuring of both transmittance and reflectance, four-parameter estimation theory is required to find their UQL [57]. Furthermore, in metamaterials, the phases and amplitudes of the transmitted light sensitively depend on the propagation direction of the incident light. In such cases, the phases need to be considered in the input-output relation of Eq. (1) if the sample is illuminated through multiple directions. In addition, the frequency-dependent response of CD would induce a further uncertainty in the measurement if a probe consists of multiple modes and cannot be approximated to a single mode. Also, various constraints on photon detectors, such as the spectral resolution or imperfect photon-number-resolving capability, need to be taken into account when predicting the magnitude of quantum enhancement. On the theoretical side, a broader investigation into global parameter estimation problems and the role of entanglement is interesting as future work.

We envision that the formalism developed and used in this work can be immediately applied to other kinds of dichroism sensing, e.g., linear dichroism sensing [13,103] or magnetic CD sensing [104,105]. The role of entanglement would be more significant when polarization conversion starts to be involved [40–43], which was not considered in this work. The CD usually occurs in units of a single photon, which enabled us to model CD by linear beam splitters. However, it may occur in units of two photons, called two-photon CD (TPCD) [106,107]. The latter needs to be modeled by nonlinear beam splitters, where transmission, reflection, and absorption take place in units of two photons. It would be interesting to study optimal TPCD sensing schemes with quantum light. CD sensing with plasmonic chiral structures is often studied [108], for which the technique studied in this work can cooperate with the recently developed quantum plasmonic sensing techniques [109–112].

APPENDIX A: QFIM FOR A COHERENT STATE INPUT

The QFIM of Eq. (12) can be rewritten as

$$H_{jk} = 4\mathrm{Re}(\langle \partial_j \Psi_{\mathrm{out}} | \partial_k \Psi_{\mathrm{out}} \rangle - \langle \partial_j \Psi_{\mathrm{out}} | \Psi_{\mathrm{out}} \rangle \langle \Psi_{\mathrm{out}} | \partial_k \Psi_{\mathrm{out}} \rangle).$$

(A1)

For the output state of Eq. (11), the derivative is written by

$$|\partial_j \Psi_{\mathrm{out}}\rangle = \sqrt{\frac{\eta_j}{4T_j}} (\alpha_j \hat{a}_j^\dagger - \alpha_j^* \hat{a}_j) |\Psi_{\mathrm{out}}\rangle,$$

(A2)

causing that the second term of Eq. (A1) vanishes for all j, k. The first term, on the other hand, is shown to be written as

$$H_{jk} = \frac{\eta_j N_j}{T_j} \delta_{jk}, \qquad (A3)$$

where δ_{jk} denotes the Kronecker delta. Thus, we have $\boldsymbol{H}$ of Eq. (14) in the main text.

APPENDIX B: SLD OPERATORS

The QFIM of Eq. (20) can be understood as the UQL to estimation of the total transmittance $\mathcal{T}_j$ of individual modes, for which the SLD operators are written as

$$\frac{\partial \hat{\rho}}{\partial \mathcal{T}_j} = \frac{1}{2}(\hat{\rho}\hat{\mathcal{L}}_j + \hat{\mathcal{L}}_j \hat{\rho}). \qquad (B1)$$

Decomposing the total transmittance as $\mathcal{T}_j = \eta_j T_j$, one can find the SLD operators $\hat{\mathcal{S}}_j$ for estimation of T_j as follows:

$$\frac{\partial \hat{\rho}}{\partial T_j} = \frac{\partial \hat{\rho}}{\partial \mathcal{T}_j}\frac{\partial \mathcal{T}_j}{\partial T_j} = \frac{\partial \hat{\rho}}{\partial \mathcal{T}_j}\eta_j = \frac{1}{2}(\hat{\rho}\hat{\mathcal{S}}_j + \hat{\mathcal{S}}_j \hat{\rho}), \qquad (B2)$$

where $\hat{\mathcal{S}}_j = \eta_j \hat{\mathcal{L}}_j$. Therefore, we have the QFIM written as

$$H_{jk} = \frac{1}{2}\mathrm{Tr}[\rho(\hat{\mathcal{S}}_j\hat{\mathcal{S}}_j + \hat{\mathcal{S}}_j\hat{\mathcal{S}}_j)] = \frac{\eta_j N_j}{T_j(1 - \eta_j T_j)}\delta_{jk}, \qquad (B3)$$

where δ_{jk} denotes the Kronecker delta. Thus, we have $\boldsymbol{H}_{\mathrm{max}}$ of Eq. (22) in the main text and this is the modified UQL to estimation of T_j in the presence of loss.

APPENDIX C: QUANTUM FIDELITY AND QFIM

An alternative way to find the QFIM is to use the relation between Bures distance $\mathcal{D}_{\mathrm{B}}^2$ [63,113,114], quantum fidelity $\mathcal{F}$ [115,116], and QFIM. In our case, the QFIM H_{jk} is related to the Bures distance $\mathcal{D}_{\mathrm{B}}^2$ for the infinitesimally close states $\hat{\rho}_{\boldsymbol{T}}$ and $\hat{\rho}_{\boldsymbol{T}+d\boldsymbol{T}}$. It can be written as [57]

$$\sum_{j,k\in\{\mathrm{L,R}\}} H_{jk}dT_j dT_k = 4\mathcal{D}_{\mathrm{B}}^2(\hat{\rho}_{\boldsymbol{T}}, \hat{\rho}_{\boldsymbol{T}+d\boldsymbol{T}}), \qquad (C1)$$

where the Bures distance can be written in terms of quantum fidelity as

$$\mathcal{D}_{\mathrm{B}}^2(\hat{\rho}_{\boldsymbol{T}}, \hat{\rho}_{\boldsymbol{T}+d\boldsymbol{T}}) = 2[1 - \sqrt{\mathcal{F}(\hat{\rho}_{\boldsymbol{T}}, \hat{\rho}_{\boldsymbol{T}+d\boldsymbol{T}})}] \qquad (C2)$$

and the quantum fidelity is defined as

$$\mathcal{F}(\hat{\rho}_{\boldsymbol{T}}, \hat{\rho}_{\boldsymbol{T}+d\boldsymbol{T}}) = \left(\mathrm{Tr}\sqrt{\sqrt{\hat{\rho}_{\boldsymbol{T}}}\hat{\rho}_{\boldsymbol{T}+d\boldsymbol{T}}\sqrt{\hat{\rho}_{\boldsymbol{T}}}}\right)^2. \qquad (C3)$$

Thus, the calculation of quantum fidelity leads to the calculation of QFIM.

For a TMSV state input, the output state $\hat{\rho}_{\boldsymbol{T}}$ can be characterized by only the second-order moments, i.e., the covariance matrix $\boldsymbol{V}$ [117,118]. Using the analytical form of quantum fidelity that has been found for covariance matrices [93,94], one can readily calculate the quantum fidelity for the TMSV state input.

The covariance matrix $\boldsymbol{V}$ is defined by $V_{jk} = \mathrm{Tr}[\hat{\rho}_{\boldsymbol{T}}\{\hat{Q}_j - d_j, \hat{Q}_k - d_k\}/2]$, where $\{\hat{A}, \hat{B}\} \equiv \hat{A}\hat{B} + \hat{B}\hat{A}$ and $d_j = \mathrm{Tr}[\hat{\rho}_{\boldsymbol{T}}\hat{Q}_j]$. Here, $\hat{\boldsymbol{Q}}$ denotes a quadrature operator vector for a two-mode continuous variable quantum system and written as $\hat{\boldsymbol{Q}} = (\hat{x}_1, \hat{p}_1, \hat{x}_2, \hat{p}_2)^{\mathrm{T}}$ satisfying the canonical commutation relation, $[\hat{Q}_j, \hat{Q}_k] = i\Omega_{jk}$, where $\Omega = \begin{pmatrix} 0 & 1 \\ -1 & 0 \end{pmatrix} \times \mathbb{I}_2$ and $\mathbb{I}_n$ is the $n \times n$ identity matrix.

For the output state $\hat{\rho}_{\boldsymbol{T}}$ for the TMSV state input, it can be shown that $\boldsymbol{d} = (0, 0, 0, 0)^{\mathrm{T}}$, while

$$\boldsymbol{V}(\boldsymbol{T}) = \begin{pmatrix} v_1 & 0 & -v_3 & 0 \\ 0 & v_1 & 0 & v_3 \\ -v_3 & 0 & v_2 & 0 \\ 0 & v_3 & 0 & v_2 \end{pmatrix}, \qquad (C4)$$

where

$$v_1 = \tfrac{1}{2} + \eta_{\mathrm{L}}T_{\mathrm{L}}\sinh^2 r, \qquad (C5)$$

$$v_2 = \tfrac{1}{2} + \eta_{\mathrm{R}}T_{\mathrm{R}}\sinh^2 r, \qquad (C6)$$

$$v_3 = \tfrac{1}{2}\sqrt{\eta_{\mathrm{L}}\eta_{\mathrm{R}}T_{\mathrm{L}}T_{\mathrm{R}}}\sinh 2r, \qquad (C7)$$

where a squeezing parameter has been assumed to be real, i.e., $\xi = r \in \mathbb{R}$.

For two states described by the covariance matrices $\boldsymbol{V}_1$ and $\boldsymbol{V}_2$ but having zero displacement, the quantum fidelity can be written as [93,94]

$$\mathcal{F}(\boldsymbol{V}_1, \boldsymbol{V}_2) = \left[\sqrt{\gamma} + \sqrt{\lambda} - \sqrt{(\sqrt{\gamma} + \sqrt{\lambda})^2 - \delta}\right]^{-1}, \qquad (C8)$$

where

$$\delta = \det(\boldsymbol{V}_1 + \boldsymbol{V}_2), \qquad (C9)$$

$$\gamma = 16\det(\Omega\boldsymbol{V}_1\Omega\boldsymbol{V}_2 - \mathbb{I}_4/4), \qquad (C10)$$

$$\lambda = 16\det(\boldsymbol{V}_1 + i\Omega/2)\det(\boldsymbol{V}_2 + i\Omega/2). \qquad (C11)$$

With the above formalism and analytical form of the quantum fidelity, one can thus derive the QFIM of Eqs. (30) and (31) in the main text.

---

[1] N. J. Greenfield, Using circular dichroism spectra to estimate protein secondary structure, Nat. Protocols **1**, 2876 (2006).

[2] A. Micsonai, F. Wien, L. Kernya, Y. Lee, Y. Goto, M. Réfrégiers, and J. Kardos, Accurate secondary structure prediction and fold recognition for circular dichroism spectroscopy, Proc. Natl. Acad. Sci. USA **112**, E3095 (2015).

[3] J. K. Gansel, M. Thiel, M. S. Rill, M. Decker, K. Bade, V. Saile, G. von Freymann, S. Linden, and M. Wegener, Gold helix photonic metamaterial as broadband circular polarizer, Science **325**, 1513 (2009).

[4] A. Passaseo, M. Esposito, M. Cuscuná, and V. Tasco, Materials and 3D designs of helix nanostructures for

chirality at optical frequencies, Adv. Opt. Mater. **5**, 1601079 (2017).

[5] J. T. Collins, C. Kuppe, D. C. Hooper, C. Sibilia, M. Centini, and V. K. Valev, Chirality and chiroptical effects in metal nanostructures: Fundamentals and current trends, Adv. Opt. Mater. **5**, 1700182 (2017).

[6] V. K. Valev, J. J. Baumberg, C. Sibilia, and T. Verbiest, Chirality and chiroptical effects in plasmonic nanostructures: Fundamentals, recent progress, and outlook, Adv. Mater. **25**, 2517 (2013).

[7] Y. Luo, C. Chi, M. Jiang, R. Li, S. Zu, Y. Li, and Z. Fang, Plasmonic chiral nanostructures: Chiroptical effects and applications, Adv. Opt. Mater. **5**, 1700040 (2017).

[8] B. Bai, Y. Svirko, J. Turunen, and T. Vallius, Optical activity in planar chiral metamaterials: Theoretical study, Phys. Rev. A **76**, 023811 (2007).

[9] S. S. Oh and O. Hess, Chiral metamaterials: Enhancement and control of optical activity and circular dichroism, Nano Convergence **2**, 24 (2015).

[10] M. Anson and P. M. Bayley, Measurement of circular dichroism at millisecond time resolution: A stopped-flow circular dichroism system, J. Phys. E: Sci. Instrum. **7**, 481 (1974).

[11] C. M. Caves, Quantum-mechanical noise in an interferometer, Phys. Rev. D **23**, 1693 (1981).

[12] R. Schnabel, N. Mavalvala, D. E. McClelland, and P. K. Lam, Quantum metrology for gravitational wave astronomy, Nat. Commun. **1**, 121 (2010).

[13] A. Rodger and B. Nordén, *Circular Dichroism and Linear Dichroism* (Oxford University Press, Oxford, 1997).

[14] S. M. Kelly, T. J. Jess, and N. C. Price, How to study proteins by circular dichroism, Biochim. Biophys. Acta, Proteins Proteomics **1751**, 119 (2005).

[15] K. C. Neuman, E. H. Chadd, G. F. Liou, K. Bergman, and S. M. Block, Characterization of photodamage to escherichia coli in optical traps, Biophys. J. **77**, 2856 (1999).

[16] E. J. G. Peterman, F. Gittes, and C. F. Schmidt, Laser-induced heating in optical traps, Biophys. J. **84**, 1308 (2003).

[17] M. Taylor, *Quantum Microscopy of Biological Systems* (Springer, Switzerland, 2015).

[18] M. A. Taylor and W. P. Bowen, Quantum metrology and its application in biology, Phys. Rep. **615**, 1 (2016).

[19] M. Hentschel, M. Schäferling, T. Weiss, N. Liu, and H. Giessen, Three-dimensional chiral plasmonic oligomers, Nano Lett. **12**, 2542 (2012).

[20] S. H. Yoo and Q. Han Park, Chiral Light-Matter Interaction in Optical Resonators, Phys. Rev. Lett. **114**, 203003 (2015).

[21] M. L. Nesterov, X. Yin, M. Schäferling, H. Giessen, and T. Weiss, The role of plasmon-generated near fields for enhanced circular dichroism spectroscopy, ACS Photonics **3**, 578 (2016).

[22] E. Mohammadi, K. L. Tsakmakidis, A. N. Askarpour, P. Dehkhoda, A. Tavakoli, and H. Altug, Nanophotonic platforms for enhanced chiral sensing, ACS Photonics **5**, 2669 (2018).

[23] F. Graf, J. Feis, X. Garcia-Santiago, M. Wegener, C. Rockstuhl, and I. Fernandez-Corbaton, Achiral, helicity preserving, and resonant structures for enhanced sensing of chiral molecules, ACS Photonics **6**, 482 (2019).

[24] J. Feis, D. Beutel, J. Köpfler, X. Garcia-Santiago, C. Rockstuhl, M. Wegener, and I. Fernandez-Corbaton, Helicity-

Preserving Optical Cavity Modes for Enhanced Sensing of Chiral Molecules, Phys. Rev. Lett. **124**, 033201 (2020).

[25] S.-J. Yoon, J.-S. Lee, C. Rockstuhl, C. Lee, and K.-G. Lee, Experimental quantum polarimetry using heralded single photons, Metrologia **57**, 045008 (2020).

[26] N. Tischler, M. Krenn, R. Fickler, X. Vidal, A. Zeilinger, and G. Molina-Terriza, Quantum optical rotatory dispersion, Sci. Adv. **2**, 1601306 (2016).

[27] C. L. Degen, F. Reinhard, and P. Cappellaro, Quantum sensing, Rev. Mod. Phys. **89**, 035002 (2017).

[28] S. Pirandola, B. R. Bardhan, T. Gehring, C. Weedbrook, and S. Lloyd, Advances in photonic quantum sensing, Nat. Photonics **12**, 724 (2018).

[29] G. Spedalieri, L. Piersimoni, O. Laurino, S. L. Braunstein, and S. Pirandola, Detecting and tracking bacteria with quantum light, Phys. Rev. Research **2**, 043260 (2020).

[30] X. Guo, C. R. Breum, J. Borregaard, S. Izumi, M. V. Larsen, M. Christandl, J. S. Neergaard-Nielsen, and U. L. Andersen, Distributed quantum sensing in a continuous variable entangled network, Nat. Phys. **16**, 281 (2020).

[31] C. Oh, C. Lee, S. H. Lie, and H. Jeong, Optimal distributed quantum sensing using Gaussian states, Phys. Rev. Research **2**, 023030 (2020).

[32] J. A. Gross and C. M. Caves, One from many: Estimating a function of many parameters, J. Phys. A: Math. Theor. **54**, 014001 (2021).

[33] J. Kołodyński and R. Demkowicz-Dobrzański, Phase estimation without *a priori* phase knowledge in the presence of loss, Phys. Rev. A **82**, 053804 (2010).

[34] M. D. Lang and C. M. Caves, Optimal Quantum-Enhanced Interferometry Using a Laser Power Source, Phys. Rev. Lett. **111**, 173601 (2013).

[35] M. Takeoka, K. P. Seshadreesan, C. You, S. Izumi, and J. P. Dowling, Fundamental precision limit of a Mach-Zehnder interferometric sensor when one of the inputs is the vacuum, Phys. Rev. A **96**, 052118 (2017).

[36] P. J. Stephens, F. J. Devlin, and J. J. Pan, The determination of the absolute configurations of chiral molecules using vibrational circular dichroism (VCD) spectroscopy, Chirality **20**, 643 (2008).

[37] J. Kypr, I. Kejnovská, D. Renčiuk, and M. Vorlíčková, Circular dichroism and conformational polymorphism of DNA, Nucleic Acids Res. **37**, 1713 (2009).

[38] A. O. Govorov, Z. Fan, P. Hernandez, J. M. Slocik, and R. R. Naik, Theory of circular dichroism of nanomaterials comprising chiral molecules and nanocrystals: Plasmon enhancement, dipole interactions, and dielectric effects, Nano Lett. **10**, 1374 (2010).

[39] F. Zhu, X. Li, Y. Li, M. Yan, and S. Liu, Enantioselective circular dichroism sensing of cysteine and glutathione with gold nanorods, Anal. Chem. **87**, 357 (2015).

[40] E. Plum, V. A. Fedotov, and N. I. Zheludev, Optical activity in extrinsically chiral metamaterial, Appl. Phys. Lett. **93**, 191911 (2008).

[41] E. Plum, V. A. Fedotov, and N. I. Zheludev, Specular optical activity of achiral metasurfaces, Appl. Phys. Lett. **108**, 141905 (2016).

[42] C. Menzel, C. Rockstuhl, and F. Lederer, Advanced Jones calculus for the classification of periodic metamaterials, Phys. Rev. A **82**, 053811 (2010).

[43] A. S. Schwanecke, V. A. Fedotov, V. V. Khardikov, S. L. Prosvirnin, Y. Chen, and N. I. Zheludev, Nanostructured metal film with asymmetric optical transmission, Nano Lett. **8**, 2940 (2008).

[44] D.-H. Kwon, P. L. Werner, and D. H. Werner, Optical planar chiral metamaterial designs for strong circular dichroism and polarization rotation, Opt. Express **16**, 11802 (2008).

[45] E. Plum, V. A. Fedotov, and N. I. Zheludev, Planar metamaterial with transmission and reflection that depend on the direction of incidence, Appl. Phys. Lett. **94**, 131901 (2009).

[46] M. Saba, M. D. Turner, K. Mecke, M. Gu, and G. E. Schröder-Turk, Group theory of circular-polarization effects in chiral photonic crystals with four-fold rotation axes applied to the eight-fold intergrowth of gyroid nets, Phys. Rev. B **88**, 245116 (2013).

[47] M. I. Khan, Z. Khalid, and F. A. Tahir, Linear and circular-polarization conversion in X-band using anisotropic metasurface, Sci. Rep. **9**, 4552 (2019).

[48] I. Fernandez-Corbaton, Forward and backward helicity scattering coefficients for systems with discrete rotational symmetry, Opt. Express **21**, 29885 (2013).

[49] C.-R. Hu, G. W. Kattawar, M. E. Parkin, and P. Herb, Symmetry theorems on the forward and backward scattering Mueller matrices for light scattering from a nonspherical dielectric scatterer, Appl. Opt. **26**, 4159 (1987).

[50] J. Kaschke, M. Blome, S. Burger, and M. Wegener, Tapered *N*-helical metamaterials with three-fold rotational symmetry as improved circular polarizers, Opt. Express **22**, 19936 (2014).

[51] X. Garcia-Santiago, S. Burger, C. Rockstuhl, and I. Fernandez-Corbaton, Measuring the electromagnetic chirality of 2d arrays under normal illumination, Opt. Lett. **42**, 4075 (2017).

[52] In general, transmission (*T*), reflection (*R*), and absorption (*A*) occur in an optical sample for a given illumination (i.e., an input state). A three-port beam splitter can model such a process. The three ports correspond to an actual mode ($\hat{a}$) for input (illumination) and output (transmission), a virtual mode ($\hat{b}$) for absorption, and a virtual mode ($\hat{d}$) for reflection, respectively. Therefore, the output operator should be described as $\hat{a}_{out} = \sqrt{T}\hat{a}_{in} + \sqrt{A}\hat{b}_{in} + \sqrt{R}\hat{d}_{in}$, where the relative phases are set for convenience. The assumption of $R = 0$ (i.e., $A = 1 - T$) together with an additional fictitious beam splitter for loss eventually leads to the input-output relation of Eq. (1).

[53] R. Loudon, *The Quantum Theory of Light* (Oxford University Press, Oxford, 2000).

[54] U. Dorner, R. Demkowicz-Dobrzanski, B. J. Smith, J. S. Lundeen, W. Wasilewski, K. Banaszek, and I. A. Walmsley, Optimal Quantum Phase Estimation, Phys. Rev. Lett. **102**, 040403 (2009).

[55] S. M. Barnett, J. Jeffers, A. Gatti, and R. Loudon, Quantum optics of lossy beam splitters, Phys. Rev. A **57**, 2134 (1998).

[56] M. Szczykulska, T. Baumgratz, and A. Datta, Multi-parameter quantum metrology, Adv. Phys.: X **1**, 621 (2016).

[57] J. Liu, H. Yuan, X.-M. Lu, and X. Wang, Quantum Fisher information matrix and multiparameter estimation, J. Phys. A: Math. Theor. **53**, 023001 (2020).

[58] A mixed input state may be considered, but it is intuitively clear and can also be rigorously shown that estimation using mixed input states performs worse than using pure input states.

[59] C. W. Helstrom, *Quantum Detection and Estimation Theory* (Academic Press, New York, 1976).

[60] M. G. A. Paris, Quantum estimation for quantum technology, Int. J. Quantum Inf. **7**, 125 (2009).

[61] S. Braunstein, How large a sample is needed for the maximum likelihood estimator to be approximately Gaussian? J. Phys. A **25**, 3813 (1992).

[62] S. S. Wilks, *Mathematical Statistics* (Wiley, New York, 1962).

[63] S. L. Braunstein and C. M. Caves, Statistical Distance and the Geometry of Quantum States, Phys. Rev. Lett. **72**, 3439 (1994).

[64] W. Ge, K. Jacobs, Z. Eldredge, A. V. Gorshkov, and M. Foss-Feig, Distributed Quantum Metrology with Linear Networks and Separable Inputs, Phys. Rev. Lett. **121**, 043604 (2018).

[65] T. Baumgratz and A. Datta, Quantum Enhanced Estimation of a Multidimensional Field, Phys. Rev. Lett. **116**, 030801 (2016).

[66] K. Matsumoto, A new approach to the Cramér-Rao-type bound of the pure-state model, J. Phys. A **35**, 3111 (2002).

[67] L. Pezze, M. A. Ciampini, N. Spagnolo, P. C. Humphreys, A. Datta, I. A. Walmsley, M. Barbieri, F. Sciarrino, and A. Smerzi, Optimal Measurements for Simultaneous Quantum Estimation of Multiple Phases, Phys. Rev. Lett. **119**, 130504 (2017).

[68] J. Rubio, P. A Knott, T. J Proctor, and J. A Dunningham, Quantum sensing networks for the estimation of linear functions, J. Phys. A: Math. Theor. **53**, 344001 (2020).

[69] P. A. Knott, T. J. Proctor, A. J. Hayes, J. F. Ralph, P. Kok, and J. A. Dunningham, Local versus global strategies in multiparameter estimation, Phys. Rev. A **94**, 062312 (2016).

[70] M. Valeri, E. Polino, D. Poderini, I. Gianani, G. Corrielli, A. Crespi, R. Osellame, N. Spagnolo, and F. Sciarrino, Experimental adaptive Bayesian estimation of multiple phases with limited data, npj Quantum Inf. **6**, 92 (2020).

[71] S. P. Nolan, A. Smerzi, and L. Pezzè, A machine learning approach to Bayesian parameter estimation, arXiv:2006.02369.

[72] R. Nair, Quantum-Limited Loss Sensing: Multiparameter Estimation and Bures Distance between Loss Channels, Phys. Rev. Lett. **121**, 230801 (2018).

[73] G. Adesso, F. Dell'Anno, S. De Siena, F. Illuminati, and L. A. M. Souza, Optimal estimation of losses at the ultimate quantum limit with non-Gaussian states, Phys. Rev. A **79**, 040305(R) (2009).

[74] B. T. H. Varcoe, S. Brattke, M. Weidinger, and H. Walther, Preparing pure photon number states of the radiation field, Nature (London) **403**, 743 (2000).

[75] P. Bertet, S. Osnaghi, P. Milman, A. Auffeves, P. Maioli, M. Brune, J. M. Raimond, and S. Haroche, Generating and Probing a Two-Photon Fock State with a Single Atom in a Cavity, Phys. Rev. Lett. **88**, 143601 (2002).

[76] E. Waks, E. Diamanti, and Y. Yamamoto, Generation of photon number states, New J. Phys. **8**, 4 (2006).

[77] B. Lounis and M. Orrit, Single-photon sources, Rep. Prog. Phys. **68**, 1129 (2005).

[78] M. D. Eisaman, J. Fan, A. Migdall, and S. V. Polyakov, Invited review article: Single-photon sources and detectors, Rev. Sci. Instrum. **82**, 071101 (2011).

[79] E. Meyer-Scott, C. Silberhorn, and A. Migdall, Single-photon sources: Approaching the ideal through multiplexing, Rev. Sci. Instrum. **91**, 041101 (2020).

[80] M. Genovese, Real applications of quantum imaging, J. Opt. **18**, 073002 (2016).

[81] S. Lloyd, Enhanced sensitivity of photodetection via quantum illumination, Science **321**, 1463 (2008).

[82] S.-H. Tan, B. I. Erkmen, V. Giovannetti, S. Guha, S. Lloyd, L. Maccone, S. Pirandola, and J. H. Shapiro, Quantum Illumination with Gaussian States, Phys. Rev. Lett. **101**, 253601 (2008).

[83] E. D. Lopaeva, I. Ruo Berchera, I. P. Degiovanni, S. Olivares, G. Brida, and M. Genovese, Experimental Realization of Quantum Illumination, Phys. Rev. Lett. **110**, 153603 (2013).

[84] R. Nair and M. Gu, Fundamental limits of quantum illumination, Optica **7**, 771 (2020).

[85] A. Meda, E. Losero, N. Samantaray, F. Scafirimuto, S. Pradyumna, A. Avella, I. Ruo-Berchera, and M. Genovese, Photon-number correlation for quantum enhanced imaging and sensing, J. Opt. **19**, 094002 (2017).

[86] O. Jedrkiewicz, Y.-K Jiang, E. Brambilla, A. Gatti, M. Bache, L. A. Lugiato, and P. Di Trapani, Detection of Sub-Shot-Noise Spatial Correlation in High-Gain Parametric Down Conversion, Phys. Rev. Lett. **93**, 243601 (2004).

[87] M. Bondani, A. Allevi, G. Zambra, M. G. A. Paris, and A. Andreoni, Sub-shot-noise photon-number correlation in a mesoscopic twin beam of light, Phys. Rev. A **76**, 013833 (2007).

[88] J.-L. Blanchet, F. Devaux, L. Furfaro, and E. Lantz, Measurement of Sub-Shot-Noise Correlations of Spatial Fluctuations in the Photon-Counting Regime, Phys. Rev. Lett. **101**, 233604 (2008).

[89] J. Peřina, M. Hamar, V. Michálek, and O. Haderka, Photon-number distributions of twin beams generated in spontaneous parametric down-conversion and measured by an intensified CCD camera, Phys. Rev. A **85**, 023816 (2012).

[90] D. C. Burnham and D. L. Weinberg, Observation of Simultaneity in Parametric Production of Optical Photon Pairs, Phys. Rev. Lett. **25**, 84 (1970).

[91] A. Heidmann, R. J. Horowicz, S. Reynaud, E. Giacobino, C. Fabre, and G. Camy, Observation of Quantum Noise Reduction on Twin Laser Beams, Phys. Rev. Lett. **59**, 2555 (1987).

[92] B. L. Schumaker and C. M. Caves, New formalism for two-photon quantum optics. II. Mathematical foundation and compact notation, Phys. Rev. A **31**, 3093 (1985).

[93] P. Marian and T. A. Marian, Uhlmann fidelity between two-mode Gaussian states, Phys. Rev. A **86**, 022340 (2012).

[94] L. Banchi, S. L. Braunstein, and S. Pirandola, Quantum Fidelity for Arbitrary Gaussian States, Phys. Rev. Lett. **115**, 260501 (2015).

[95] S. M. Kay, *Fundamentals of Statistical Signal Processing: Estimation Theory* (Prentice Hall, New York, 1993).

[96] C. Oh, C. Lee, C. Rockstuhl, H. Jeong, J. Kim, H. Nha, and S. Lee, Optimal Gaussian measurements for phase estimation in single-mode Gaussian metrology, npj Quantum Inf. **5**, 10 (2019).

[97] I. Holzman and Y. Ivry, Superconducting nanowires for single-photon detection: Progress, challenges, and opportunities, Adv. Quantum Technol. **2**, 1800058 (2019).

[98] R. Whittaker, C. Erven, A. Neville, M. Berry, J. L. O'Brien, H. Cable, and J. C. F. Matthews, Absorption spectroscopy at the ultimate quantum limit from single-photon states, New J. Phys. **19**, 023013 (2017).

[99] P.-A. Moreau, J. Sabines-Chesterking, R. Whittaker, S. K. Joshi, P. M. Birchall, A. McMillan, J. G. Rarity, and J. C. F. Matthews, Demonstrating an absolute quantum advantage in direct absorption measurement, Sci. Rep. **7**, 6256 (2017).

[100] E. Losero, I. Ruo-Berchera, A. Meda, A. Avella, and M. Genovese, Unbiased estimation of an optical loss at the ultimate quantum limit with twin-beams, Sci. Rep. **8**, 7431 (2018).

[101] F. Dell'Anno, S. De Siena, and F. Illuminati, Multiphoton quantum optics and quantum state engineering, Phys. Rep. **428**, 53 (2006).

[102] O. S. Magaña-Loaiza, R. de J. León-Montiel, A. Perez-Leija, A. B. U'Ren, C. You, K. Busch, A. E. Lita, S. W. Nam, R. P. Mirin, and T. Gerrits, Multiphoton quantum-state engineering using conditional measurements, npj Quantum Inf. **5**, 80 (2019).

[103] F. Dörr, Spectroscopy with polarized light, Angew. Chem., Int. Ed. **5**, 478 (1966).

[104] P. J. Stephens, Theory of magnetic circular dichroism, J. Chem. Phys. **52**, 3489 (1970).

[105] C. T. Chen, Y. U. Idzerda, H.-J. Lin, N. V. Smith, G. Meigs, E. Chaban, G. H. Ho, E. Pellegrin, and F. Sette, Experimental Confirmation of the X-Ray Magnetic Circular Dichroism Sum Rules for Iron and Cobalt, Phys. Rev. Lett. **75**, 152 (1995).

[106] I. Tinoco Jr., Two-photon circular dichroism, J. Chem. Phys. **62**, 1006 (1975).

[107] E. A. Power, Two-photon circular dichroism, J. Chem. Phys. **63**, 1348 (1975).

[108] H.-H. Jeong, A. G. Mark, M. Alarcón-Correa, I. Kim, P. Oswald, T.-C. Lee, and P. Fischer, Dispersion and shape engineered plasmonic nanosensors, Nat. Commun. **7**, 11331 (2016).

[109] W. Fan, B. J. Lawrie, and R. C. Pooser, Quantum plasmonic sensing, Phys. Rev. A **92**, 053812 (2015).

[110] C. Lee, F. Dieleman, J. Lee, C. Rockstuhl, S. A. Maier, and M. Tame, Quantum plasmonic sensing: Beyond the shot-noise and diffraction limit, ACS Photonics **3**, 992 (2016).

[111] C. Lee, M. Tame, C. Rockstuhl, and K.-G. Lee, Introduction to quantum plasmonic sensing, in *Nano-Optics: Fundamentals, Experimental Methods, and Applications*, edited by S. Thomas, Y. Grohens, G. Vignaud, N. Kalarikkal, and J. James (Elsevier, Amsterdam, 2020), Chap. 5, pp. 67–112.

[112] C. Lee, B. Lawrie, R. Pooser, K.-G. Lee, C. Rockstuhl, and M. Tame, Quantum plasmonic sensors, Chem. Rev. **121**, 4743 (2021).

[113] D. Bures, An extension of Kakutani's theorem on infinite product measures to the tensor product of semifinite $w*$-algebras, Trans. Am. Math. Soc. **135**, 199 (1969).

[114] P. Facchi, R. Kulkarni, V. I. Manko, G. Marmo, E. C. G. Sudarshan, and F. Ventriglia, Classical and quantum Fisher information in the geometrical formulation of quantum mechanics, Phys. Lett. A **374**, 4801 (2010).

[115] A. Uhlmann, The "transition probability" in the state space of a $w*$-algebra, Rep. Math. Phys. **9**, 273 (1976).

[116] R. Jozsa, Fidelity for mixed quantum states, J. Mod. Opt. **41**, 2315 (1994).

[117] S. L. Braunstein and P. van Loock, Quantum information with continuous variables, Rev. Mod. Phys. **77**, 513 (2005).

[118] C. Weedbrook, S. Pirandola, R. Garcia-Patron, N. J. Cerf, T. C. Ralph, J. H. Shapiro, and S. Lloyd, Gaussian quantum information, Rev. Mod. Phys. **84**, 621 (2012).